



# Superconvergence and the Numerical Flux: a Study Using the Upwind-Biased Flux in Discontinuous Galerkin Methods

Daniel J. Frean<sup>1</sup> · Jennifer K. Ryan<sup>1,2</sup>

Received: 3 April 2019 / Revised: 2 October 2019 / Accepted: 5 October 2019 / Published online: 7 December 2019  
© The Author(s) 2019

## Abstract

One of the beneficial properties of the discontinuous Galerkin method is the accurate wave propagation properties. That is, the semi-discrete error has dissipation errors of order  $2k + 1$  ( $\leq Ch^{2k+1}$ ) and order  $2k + 2$  for dispersion ( $\leq Ch^{2k+2}$ ). Previous studies have concentrated on the order of accuracy, and neglected the important role that the error constant,  $C$ , plays in these estimates. In this article, we show the important role of the error constant in the dispersion and dissipation error for discontinuous Galerkin approximation of polynomial degree  $k$ , where  $k = 0, 1, 2, 3$ . This gives insight into why one may want a more centred flux for a piecewise constant or quadratic approximation than for a piecewise linear or cubic approximation. We provide an explicit formula for these error constants. This is illustrated through one particular flux, the upwind-biased flux introduced by Meng et al., as it is a convex combination of the upwind and downwind fluxes. The studies of wave propagation are typically done through a Fourier ansatz. This higher order Fourier information can be extracted using the smoothness-increasing accuracy-conserving (SIAC) filter. The SIAC filter ties the higher order Fourier information to the negative-order norm in physical space. We show that both the proofs of the ability of the SIAC filter to extract extra accuracy and numerical results are unaffected by the choice of flux.

**Keywords** Discontinuous Galerkin · Smoothness-increasing accuracy-conserving (SIAC) filtering · Superconvergence

**Mathematics Subject Classification** 65M60

---

Daniel J. Frean and Jennifer K. Ryan: Supported by the Air Force Office of Scientific Research (AFOSR), Air Force Material Command, USAF, under Grant number FA8655-13-1-3017.

---

✉ Jennifer K. Ryan  
jkryan@mines.edu

<sup>1</sup> School of Mathematics, University of East Anglia, Norwich, UK

<sup>2</sup> Applied Mathematics and Statistics, Colorado School of Mines, Golden, CO, USA

## 1 Introduction

There have been many studies on the accurate wave propagation properties for discontinuous Galerkin methods [3, 9, 10, 14, 19, 21, 24, 25]. These studies conclude that, in general, the semi-discrete error has dissipation errors of order  $2k + 1$  ( $\leq Ch^{2k+1}$ ) and order  $2k + 2$  ( $\leq Ch^{2k+2}$ ) for dispersion. These studies concentrate on the order of the error and ignore the role of the error constant. In this article, we give an explicit formula for how the error constant in the dispersion and dissipation error depends on the numerical flux as well as the polynomial degree. Specifically, when using a piecewise constant or quadratic approximation, the results suggest that one should use a more central flux to optimise the numerical wave propagation properties. For a piecewise linear or cubic approximation, the results confirm that an upwind flux is desirable. These results are illustrated through the use of the upwind-biased flux introduced by Meng et al. [15], which uses a convex combination of the upwind and downwind approximation values. In addition to this result, we introduce results for post-processing the numerical solution using the smoothness-increasing accuracy-conserving (SIAC) filter by Ryan and others [11–13, 18, 20]. This filter allows for extracting the higher order Fourier information that is used in the proof of the dissipation and dispersion errors and translates this information into physical space. To complete our discussion of superconvergence, we also review the pointwise superconvergence results for of Cao et al. [5] for the upwind-biased flux.

To summarize the contribution of this article, it is to (i) show the important role the error constant plays in the dissipation and dispersion error and its significance in tying the choice of flux to even versus odd polynomial degree approximations; (ii) show how this Fourier-type information can be extracted via SIAC filters; and (iii) tie the superconvergent information together through a review of pointwise superconvergent results.

The discontinuous Galerkin (DG) methods are one of the most extensively researched classes of numerical methods for solving partial differential equations that display convective or diffusive qualities and have been popularly adopted by the scientific and engineering communities as a method capable of achieving arbitrary orders of accuracy in space. The choice of the numerical flux function plays a pivotal role in the successful construction of DG methods and has an intrinsic effect on the superconvergence properties. The vast majority of theory for DG schemes for conservation laws has been developed with the (somewhat habituated) choice of a monotone numerical flux. Design and criteria for the selection of numerical flux functions is an area with a great deal of scope for further investigation. One approach is to not only explore the order of the dissipation and dispersion errors, but also the error constant to ensure that the errors from dispersion and dissipation are minimized.

For a Runge–Kutta (RK) DG solution to the linear advection equation, one can do better than the “natural” upwind flux. Recently, Meng et al. [15] introduced in the context of DG methods for linear hyperbolic equations a more general flux function: the upwind-biased flux. This function parametrises the ratio of information taken from the left compared to the right of cell interfaces. This choice avoids the requirement of exact knowledge of the eigenstructure of the Jacobian and may reduce numerical dissipation (yielding a better approximation in smooth regions) but it is made at the cost of the loss of monotonicity. These results provide the theoretical foundations for our investigations into the choice of flux function for RK–DG methods.

Recent interest [3, 9, 10, 14, 19, 21, 24, 25] in analysis via a Fourier approach of DG solutions to the linear advection equation offers an alternative means by which to explore superconvergence. This analysis is limited to linear equations with periodic boundary conditions and a uniform mesh. However, as is justified by numerical examples [9], the results provide a guide for the behaviour of solutions in a more general

setting. Stability and  $(k + 1)$ -th order accuracy can be established via this approach. Furthermore, this analysis is useful for exploring the time propagation of errors. In [9], it was shown that a  $k$ th-order DG solution to the linear advection equation has one physical mode and  $k$  spurious ones which are damped exponentially fast over time,

$$\|e\| \leq C_1 T h^\sigma + C_2 h^{k+1} + C_3 \exp\left(-C \frac{T}{h}\right) h^{k+1}, \quad (1)$$

where  $C_1, C_2, C_3, C \in \mathbb{R}_+$ . The first term on the right-hand side of inequality (1), which dominates for  $T = \mathcal{O}(1/h^{\sigma-k-1})$ , is attributed to the dispersion and dissipation errors of the physically relevant eigenvalues and grows linearly in time. The expected order of accuracy is  $\sigma = k + 1$ ; however, a judicious choice of the numerical flux function in the semi-discrete DG scheme can yield a superconvergent order of accuracy as high as  $\sigma = 2k + 1$ . The third term, which decays exponentially fast over time with respect to  $h$ , accounts for dissipation of the spurious modes. The second term is due to projection of the initial condition and does not grow in time. Thus the error is on the order of  $2k + 1$  for long time integration but only  $k + 1$  over short time. At certain special points (the superconvergent points which change with the choice of numerical flux) the accuracy of inequality (1) can be increased to  $\mathcal{O}(h^{p+2})$  by carefully interpolating the initial projection.

The above superconvergence results can be extracted from the underlying approximation to achieve  $2k + 1$  in the  $\mathcal{L}^2$ -norm. This involves convolving the approximation against a specially designed kernel comprising a linear combination of B-splines [7, 11, 12, 18, 20], effecting increased smoothness by damping the non-physical eigenmodes of the DG operator and exploiting information concealed in the unwelcome fluctuations that characterise the numerical solution. We are able to extend the analysis of the SIAC filtered error, which is facilitated by a dual analysis in a similar fashion to [12] for the case of the upwind-biased flux and is limited to a contribution to the constant attached to the post-processed error term.

The outline of this paper is as follows: in Sect. 2, we discuss the preliminaries needed to perform both the pointwise and negative-order norm error analysis as well as reviewing the upwind-biased DG scheme. This includes a review of the pointwise superconvergent results for the upwind-biased DG scheme. In Sect. 3 we discuss the dispersion analysis related to this scheme and how the constants depend on the choice of the upwind biasing in the flux. In Sect. 4 we extend the negative-order norm error analysis to upwind-biased DG schemes and show that this simply affects the constant in the error. We end by supporting this analysis with numerical examples in Sect. 5 and conclusions in Sect. 6.

## 2 Preliminaries

We begin with some definitions used in the error estimates for discontinuous Galerkin solutions and SIAC filtering and complete the prefatory construction of the DG scheme.

### 2.1 Notation and Definitions

We first treat the discretisation of a multi-dimensional spatial domain and define the associated approximation spaces.

Consider the linear hyperbolic system

$$u_t + \sum_{i=1}^d a_i u_{x_i} = 0, \quad (\mathbf{x}, t) \in \Omega \times (0, T] \tag{2}$$

for the conserved quantity  $u(\mathbf{x}, t)$ , where  $\mathbf{x} = (x_1, \dots, x_d) \in \Omega \subset \mathbb{R}^d$  and where we assume that we have real constant coefficients  $a_i \geq 0$ . We adopt throughout this paper the assumptions of a smooth initial condition and of periodicity in the boundary conditions:

$$u(\mathbf{x}, 0) = u_0(\mathbf{x}) \in \mathcal{C}^\infty(\Omega); \quad u(\mathbf{x}, 0) = u(\mathbf{x}, T).$$

For much of the error analyses, it is required only that  $u_0(\mathbf{x}) \in \mathcal{H}^{k+1}(\Omega)$  but for the proof of Theorem 2.3, we require infinite differentiability to write the DG solution as a Maclaurin series.

### 2.1.1 Tessellation

Let  $\Omega_h$  be a tessellation of a  $d$ -dimensional bounded domain  $\Omega$  into elements  $S$  of the regular quadrilateral-type shape. Denote by  $\partial\Omega_h = \bigcup_{S \in \Omega_h} \partial S$  the union of boundary faces  $\partial S$  of the elements  $S \in \Omega_h$ . A face  $e$  internal to the domain has associated with the “left” and “right” elements  $S_L$  and  $S_R$  and exterior-pointing normal vectors  $\mathbf{n}_L = (n_1^L, \dots, n_d^L)$  and  $\mathbf{n}_R = (n_1^R, \dots, n_d^R)$ , respectively, as described in [12]. Given a function  $v$  defined on neighbouring elements  $S_L$  and  $S_R$  which share a face  $e$ , we refer to its restriction in  $S_L$  to the face  $e$  by writing  $v^L := (v|_{S_L})|_e$  and similarly for  $v^R$ , the restriction of  $v$  to  $e$  in  $S_R$ .

For clarity, we detail the discretisation of a two-dimensional domain  $\Omega = [-1, 1]^2$  into  $N_x \cdot N_y$  rectangular cells. Elements take the form  $S = I_i \times J_j$  where  $I_i$  and  $J_j$  are intervals given by

$$I_i = \left(x_{i-\frac{1}{2}}, x_{i+\frac{1}{2}}\right) \quad \text{and} \quad J_j = \left(y_{j-\frac{1}{2}}, y_{j+\frac{1}{2}}\right)$$

for  $1 \leq i \leq N_x$  and  $1 \leq j \leq N_y$  respectively, where

$$-1 = x_{\frac{1}{2}} < x_{\frac{3}{2}} < \dots < x_{N_x+\frac{1}{2}} = 1$$

and

$$-1 = y_{\frac{1}{2}} < y_{\frac{3}{2}} < \dots < y_{N_y+\frac{1}{2}} = 1.$$

Denoting by  $h_{x,i} = x_{i+\frac{1}{2}} - x_{i-\frac{1}{2}}$ ,  $1 \leq i \leq N_x$ , and  $h_{y,j} = y_{j+\frac{1}{2}} - y_{j-\frac{1}{2}}$ ,  $1 \leq j \leq N_y$ , we define

$$h = \max \left\{ \max_{1 \leq i \leq N_x} h_{x,i}, \max_{1 \leq j \leq N_y} h_{y,j} \right\}$$

and require regularity:  $h_{x,i}, h_{y,j} \geq ch$ ,  $c > 0$ . For simplicity of the filtered error estimates in Sect. 4, and by necessity in Sect. 3, we will adopt constant element lengths

$$x_{i+\frac{1}{2}} - x_{i-\frac{1}{2}} = h_x, \quad y_{j+\frac{1}{2}} - y_{j-\frac{1}{2}} = h_y$$

for all  $i$  and  $j$ . On an element  $S = I_i \times J_j$ , evaluation of functions  $v$  at cell boundary points of the form  $(x_{i+\frac{1}{2}}, y)$ , for example, is written as

$$v^L|_{x=x_{i+\frac{1}{2}}} = v\left(x_{i+\frac{1}{2}}^-, y\right).$$

### 2.1.2 Basis Polynomials

We use as basis functions the Legendre polynomials  $P_n(\xi)$ , which can be defined by the Rodrigues formula

$$P_n(\xi) = \frac{1}{2^n n!} \frac{d^n}{d\xi^n} ((\xi^2 - 1)^n), \quad -1 \leq \xi \leq 1,$$

and which satisfy the orthogonality condition

$$\int_{-1}^1 P_n(\xi) P_m(\xi) d\xi = \frac{2}{2n + 1} \delta_{nm},$$

where  $\delta_{nm}$  is the Kronecker-delta function. We can then define the right and left Radau polynomials as

$$R_{k+1}^+(\xi) = P_{k+1}(\xi) - P_k(\xi), \quad R_{k+1}^-(\xi) = P_{k+1}(\xi) + P_k(\xi),$$

respectively. It is known that the roots

$$\xi_1^+ < \xi_2^+ < \dots < \xi_{k+1}^+ = 1$$

of  $R_{k+1}^+(\xi)$  and the roots

$$-1 = \xi_1^- < \xi_2^- < \dots < \xi_{k+1}^-$$

of  $R_{k+1}^-(\xi)$  are real, distinct and lie in the interval  $[-1, 1]$ .

### 2.1.3 Function Spaces

Due to the tensor product nature of the post-processing kernel, we will require the function space of tensor product polynomials  $\mathcal{P}^k(S)$  of degree at most  $k$  in each variable. Thus, we base the proofs in this paper on the following finite element spaces:

$$\begin{aligned} V_h^k &= \{ \phi \in \mathcal{L}^2(\Omega) : \phi|_S \in \mathcal{P}^k(S), \forall S \in \Omega_h \} \\ \Sigma_h^k &= \{ \boldsymbol{\eta} = (\eta_1, \dots, \eta_d)^T \in (\mathcal{L}^2(\Omega))^d : \eta_l \in \mathcal{P}^k(S), \\ &\quad l = 1, \dots, d; \forall S \in \Omega_h \}, \end{aligned}$$

where  $\mathcal{L}^2(\Omega)$  is the space of square-integrable functions on  $\Omega$ . Nevertheless, we mention here that it has been observed ([18]) that the filter also works for the standard polynomial space  $\mathcal{P}^k(S)$ . Note that for a one-dimensional domain  $\Omega$ , these function spaces  $\mathcal{P}^k(S)$  and  $\mathcal{P}^k(S)$  agree.

### 2.1.4 Operators on the Function Spaces

We list the following standard notations. The inner-product over  $\Omega$  of two functions is defined as

$$(w, v)_\Omega = \sum_S \int_S wv \, dS; \quad (\mathbf{p}, \mathbf{q})_\Omega = \sum_S \int_S \mathbf{p} \cdot \mathbf{q} \, dS$$

depending on whether the functions take scalar or vector values. We denote by  $\mathbb{P}_h v$  and by  $\Pi_h \mathbf{p}$  the usual  $\mathcal{L}^2$ -projections of scalar and vector valued functions  $v$  and  $\mathbf{p}$ , respectively.

The  $\mathcal{L}^2$ -norm on the domain  $\Omega$  and on the boundary  $\partial\Omega$  is defined as

$$\|\eta\|_\Omega = \left( \int_\Omega \eta^2 \, dx \right)^{1/2}; \quad \|\eta\|_{\partial\Omega} = \left( \int_{\partial\Omega} \eta^2 \, ds \right)^{1/2}$$

and the  $\ell$ -norm and semi-norm of the Sobolev space  $H^\ell(\Omega)$  are defined, respectively, as

$$\|\eta\|_{\ell,\Omega} = \left( \sum_{|\alpha|=\ell} \|D^\alpha \eta\|_\Omega^2 \right)^{1/2}; \quad |\eta|_{\ell,\Omega} = \sum_{|\alpha|=\ell} \|D^\alpha \eta\|_{\infty,\Omega}, \quad \ell > 0,$$

where  $\alpha$  is a  $d$ -dimensional multi-index of order  $|\alpha|$  and where  $D^\alpha$  denotes multi-dimensional partial derivatives. The definitions for the above norms for vector-valued functions are analogous to the scalar case.

In Sect. 4, we will utilise the negative-order Sobolev norm, defined as

$$\|\eta\|_{-\ell,\Omega} = \sup_{\Phi \in \mathcal{C}_0^\infty(\Omega)} \frac{(\eta, \Phi)_\Omega}{\|\Phi\|_{\ell,\Omega}},$$

as a means of obtaining  $\mathcal{L}^2$ -error estimates for the filtered solution. Note that for all  $\ell \geq 1$ , we have

$$\|\eta\|_{-\ell,\Omega} \leq \|\eta\|_{\ell,\Omega}.$$

The negative order norm can be used to detect oscillations of a function [7] and is connected to the SIAC filter which smooths oscillations in the error.

Finally, the difference quotients  $\partial_{h,j} v$  are given by

$$\partial_{h,j} v(\mathbf{x}) = \frac{1}{h} \left[ v\left(\mathbf{x} + \frac{1}{2} h \mathbf{e}_j\right) - v\left(\mathbf{x} - \frac{1}{2} h \mathbf{e}_j\right) \right],$$

where  $\mathbf{e}_j$  is the  $j$ th component unit normal vector. For any multi-index  $\alpha = (\alpha_1, \dots, \alpha_d)$ , we define the  $\alpha$ th-order difference quotient by

$$\partial_{h,j}^\alpha v(\mathbf{x}) = \left( \partial_{h,1}^{\alpha_1} \dots \partial_{h,d}^{\alpha_d} \right) v(\mathbf{x}).$$

## 2.2 Discontinuous Galerkin Discretisation of the Linear Hyperbolic Conservation Law in Multiple Dimensions

### 2.2.1 Construction of the DG Scheme

Given a tessellation  $\Omega_h$  of the domain  $\Omega$ , the method is facilitated by multiplying Eq. (2) by a test function  $v$  and integrating by parts over an arbitrary element  $S \in \Omega_h$  to obtain

$$\int_S u_t v \, dS - \sum_{i=1}^d \int_S f_i(u) v_{x_i} \, dS + \sum_{i=1}^d \int_{\partial S} f_i(u) v n_i \, ds = 0. \tag{3}$$

Next, we define the piecewise polynomial approximation space as

$$V_h^k := \{v \in \mathcal{L}^2(\Omega) : v|_S \in \mathcal{L}^k(S), \forall S \in \Omega_h\}.$$

Note that functions  $v \in V_h^k$  are allowed to be discontinuous across element boundaries. This is the distinguishing feature of DG schemes amongst finite element methods.

By replacing in Eq. (3) the solution  $u(\mathbf{x}, t)$  by a numerical approximation  $u_h(\mathbf{x}, t)$  such that  $u_h(\cdot, t) \in V_h^k$ , we obtain the DG method: find, for any  $v \in V_h^k$  and for all elements  $S$ , the unique function  $u_h(\cdot, t) \in V_h^k$  which satisfies

$$\int_S (u_h)_t v \, dS - \sum_{i=1}^d \int_S f_i(u_h) v_{x_i} \, dS + \sum_{i=1}^d \int_{\partial S} \hat{f}_i(u_h) v n_i \, ds = 0, \tag{4}$$

where  $\hat{f}$  is a single-valued numerical flux function used to enforce weak continuity at the cell interfaces.

The initial condition  $u_h(\mathbf{x}, 0) \in V_h^k$  is usually taken to be the  $\mathcal{L}^2$ -projection  $\mathbb{P}_h u_0$ , although the analysis in Sect. 2.3 favours a function which interpolates  $u(\mathbf{x}, 0)$  at the superconvergent points.

Summing Eq. (4) over the elements  $S$ , we get a compact expression for the global scheme:

$$((u_h)_t, v)_{\Omega_h} + B(u_h; v) = 0,$$

where we define for future use

$$B(u_h; v) := - \sum_{i=1}^d (f_i(u_h), v_{x_i})_{\Omega_h} + \sum_{i=1}^d (\hat{f}_i(u_h), v)_{\partial\Omega_h}. \tag{5}$$

**Remark 2.1** We note that although this article considers the semi-discrete form of the DG method, the results of this article extend to fully discrete schemes such as the Lax–Wendroff DG method, provided the higher order derivatives of the fluxes are discretized using the LDG formulation as in.

### 2.2.2 Flux Function

To ensure stability of the scheme (4), it remains to define the numerical flux functions  $\hat{f}$  featured in the cell boundary terms. In general,  $\hat{f}(u_h^L, u_h^R)$  depends on values of the

numerical solution from both sides of the cell interface. Traditionally [8], this function is chosen to be a so-called monotone flux, such as the Lax–Friedrichs flux, which satisfies the Lipschitz continuity, consistency ( $\hat{f}(u, u) = f(u)$ ) and monotonicity ( $\hat{f}(\uparrow, \downarrow)$ ). For our test Eq. (2), where the linear flux  $f(u) = au$  determines a single wind direction, the usual choice in the literature is to satisfy the upwinding condition. In this paper, where  $\hat{f}(u_h) = a\hat{u}_h$ , we choose instead the upwind-biased flux

$$\hat{u}_h = \theta u_h^- + (1 - \theta)u_h^+, \quad \frac{1}{2} < \theta \leq 1, \tag{6}$$

defined here in the one-dimensional case with periodic boundary conditions, which was recently described in the context of DG methods by Meng et al. [15]. More information is taken from the left than from the right of cell boundaries and, when  $\theta = 1$ , the upwind-biased flux reduces to the purely upwind flux  $u_h^-$ . We do not allow  $\theta = \frac{1}{2}$ , which gives a central flux, since then the scheme becomes unstable.

For clarity, we particularise the evaluation of this flux at cell boundary points. In two dimensions, the upwind-biased flux

$$\hat{u}_h = \theta u_h^L + (1 - \theta)u_h^R, \quad \theta = (\theta_1, \theta_2), \quad \frac{1}{2} < \theta_1, \theta_2 \leq 1 \tag{7}$$

takes the form

$$\hat{u}_h|_{x=x_{i+\frac{1}{2}}} = \theta_1 u_h(x_{i+\frac{1}{2}}^-, y) + (1 - \theta_1)u_h(x_{i+\frac{1}{2}}^+, y) \quad \text{at } (x_{i+\frac{1}{2}}, y),$$

where  $\theta_1 > \frac{1}{2}$ , and, similarly for  $\theta_2 > \frac{1}{2}$ ,

$$\hat{u}_h|_{y=y_{j+\frac{1}{2}}} = \theta_2 u_h(x, y_{j+\frac{1}{2}}^-) + (1 - \theta_2)u_h(x, y_{j+\frac{1}{2}}^+) \quad \text{at } (x, y_{j+\frac{1}{2}}).$$

Choosing, over the upwinding principle, the upwind biased flux offers several rewards [15]: a possibly reduced numerical viscosity and easier construction, for example. However, as a price paid for introducing the parameter  $\theta$ , we sacrifice the established property of monotonicity of the flux function. In this paper, we consider in terms of superconvergence the severity of this loss of monotonicity.

### 2.3 Pointwise Superconvergence

In this subsection, we review current literature for the upwind-biased flux for DG methods [5]. In this case, the leading order term in the error is proportional to a sum, dependent upon  $\theta$ , of left and right Radau polynomials. The main result, Theorem 2.3, is an extension of the observation, for example of Adjerd et al. [1, 2], that the superconvergent points for the purely upwind DG scheme are generated by roots of right Radau polynomials. To be able to illustrate this idea, a “special” Radau polynomial can be defined as

$$R_{k+1}^*(\xi) := \theta R_{k+1}^+(\xi) + (-1)^k (1 - \theta)R_{k+1}^-(\xi). \tag{8}$$

The main idea is that the roots of  $R_{k+1}^*(\xi)$ , which change with the value of  $\theta$ , generating superconvergent points on the order of  $h^{k+2}$  in the element interior for the upwind-biased scheme.



**Remark 2.2** For odd polynomial degree  $k$ , one of these “superconvergent points” lies outside the element  $[-1, 1]$  when  $\theta < 1$ . The Legendre polynomials, which are used to construct the Radau polynomials, are defined only on the interval  $[-1, 1]$ . To determine the number of roots of  $R_{k+1}^*(\xi)$  which lie within the canonical element, the definition of Legendre polynomials are extended beyond the element boundaries. Of course, any root that we find to be outside  $[-1, 1]$  will not directly manifest itself as a superconvergent point of the DG solution.

The following Lemma describing the roots of  $R_{k+1}^*(\xi)$  is given. For this argument, it is necessary to temporarily relax the domain of definition of Legendre polynomials. That is, consider the polynomials  $P_n(\xi)$  arising from the Rodrigues formula and then extend their domain of definition to  $[-M, M]$  for some fixed, sufficiently large  $M > 0$ .

**Lemma 2.1** *Let  $k \in \mathbb{N}$  and consider*

$$R_{k+1}^*(\xi) = \theta R_{k+1}^+(\xi) + (-1)^k(1 - \theta)R_{k+1}^-(\xi), \quad \xi \in \mathbb{R}$$

with  $\theta \in (\frac{1}{2}, 1)$ . When  $k$  is even, all  $k + 1$  roots lie in the interval  $[-1, 1]$ . When  $k$  is odd, exactly one root of  $R_{k+1}^*(\xi)$  is greater than 1 while all other roots lie in the interval  $[-1, 1]$ .

**Remark 2.3** Recall that when  $\theta = 1$ , one of the superconvergent points is the downwind end  $\xi_{k+1}^* = \xi_{k+1}^+ = 1$ . When  $k$  is even, the superconvergent points shift to the left with decreasing values of  $\theta < 1$ . On the other hand, when  $k$  is odd, the points shift to the right and  $\xi_{k+1}^* > 1$ . For example, when  $k = 1$ , the roots of  $R_{k+1}^*(\xi)$  are given by

$$\xi_{1,2} = \frac{1 \mp \sqrt{1 - 3\theta + 3\theta^2}}{3(2\theta - 1)}.$$

Shown in Table 1 are approximate values of the roots of  $R_{k+1}^*(\xi)$  for two values of  $\theta$ . One can observe that for the lower value of  $\theta$ , the roots shift to the left or right depending on  $k$  and that, for  $k = 1$  and  $k = 3$ , one of the roots is indeed greater than 1.

Following the lines of [1, 5] interpolates the initial condition at roots of  $R_{k+1}^*(\xi)$ , where  $k$  is even. Lemma 2.1 dictates that it is not possible to obtain in the same way a  $k$ th degree polynomial interpolating  $u$  at all  $k + 1$  roots of  $R_{k+1}^*(\xi)$  when  $k$  is odd; there are only  $k$  roots inside  $[-1, 1]$ . Instead, one can needs to define a global projection. Here, we provide a restatement of Lemma 3.5 in [5].

**Table 1** Approximations to roots  $\xi_j^*$  ( $j = 1, \dots, k + 1$ ) of  $R_{k+1}^*(\xi)$  when  $\theta = 1$  and when  $\theta = 0.75$

$k$	$\xi_j^* = \xi_j^+$ when $\theta = 1$				$\xi_j^*$ when $\theta = 0.75$					
1	$-\frac{1}{3}$	1			-0.21	1.54				
2	-0.68	0.28	1		-0.72	0.16	0.86			
3	-0.82	-0.18	0.57	1	-0.80	-0.11	0.69	1.36		
4	-0.88	-0.44	0.16	0.72	1	-0.89	-0.48	0.09	0.62	0.93

**Lemma 2.2** *Let  $u \in \mathcal{C}^{k+1}([0, h])$ . Let  $\xi_j^* \in [-1, 1]$  ( $j = 1, \dots, k + 1$ ) be the roots of*

$$R_{k+1}^*(\xi) = \theta R_{k+1}^+(\xi) + (1 - \theta)R_{k+1}^-(\xi), \quad \xi \in [-1, 1].$$

*Denote by*

$$\pi^* u(x) = \sum_{n=1}^{k+1} L_n(x), \quad x \in [0, h]$$

*where*

$$L_n(x) = u(x_n^*) \prod_{\substack{j=1 \\ j \neq n}}^{k+1} \frac{x - x_j^*}{x_n^* - x_j^*},$$

*the  $k$ th degree Lagrange polynomial interpolating  $u$  at the (distinct) roots  $x_j^* = \frac{h}{2}(\xi_j^* + 1)$  ( $j = 1, \dots, k + 1$ ) of the shifted special Radau polynomial  $R_{k+1}^*(x)$  on  $[0, h]$ . Then, the interpolation error satisfies*

$$u(x(\xi)) - \pi^* u(x(\xi)) = h^{k+1} c_{k+1} R_{k+1}^*(\xi) + \sum_{\ell=k+2}^{\infty} Q_\ell(\xi) h^\ell, \tag{9}$$

*where  $Q_\ell(\xi)$  is a polynomial of degree at most  $\ell$ .*

The interpolatory polynomials described in Lemma 2.2 are used as initial conditions in the proof of Theorem 2.3. Numerical results in Sect. 5 confirm that, in general, there are only  $k$  superconvergent points in each element when  $k$  is odd.

Here, we provide a restatement of Lemma 3.8 in [5] and Theorem 3.12.

**Theorem 2.3** *Consider the approximate solution  $u_h$  to the one-dimensional linear hyperbolic conservation law (2) with  $d = 1$  obtained by a DG scheme (4) using  $k$ th order basis functions, a uniform mesh and the upwind-biased flux  $\hat{u}_h$ . Let the numerical initial condition be the interpolating polynomial  $\pi^* u(x, 0)$  described in Lemma 2.2.*

*Let  $\xi = \frac{2}{h}x - \frac{1}{h}(x_{j+\frac{1}{2}} + x_{j-\frac{1}{2}})$  be the scaling between the cell  $I_j$  and the canonical element  $[-1, 1]$ . Then, the error  $e = u - u_h$  satisfies*

$$e(\xi, h, t) = \sum_{\ell=k+1}^{\infty} Q_\ell(\xi, t) h^\ell, \quad Q_\ell(\cdot, t) \in \mathcal{P}^\ell([-1, 1]) \tag{10}$$

*with*

$$Q_{k+1}(\xi, t) = c_{k+1}R_{k+1}^*(\xi) = c_{k+1}(\theta R_{k+1}^+(\xi) + (1 - \theta)R_{k+1}^-(\xi)),$$

where  $c_{k+1}$  depends on  $u, h, k$  and  $t$ .

**Remark 2.4** When  $u_h(x, 0) = \pi^*u_0(x)$  interpolates  $u_0(x)$  at the roots of  $R_{k+1}^*(x)$ , the coefficient of the term on the order of  $h^{k+1}$  in the series for the initial error satisfies

$$\theta Q_{k+1}(1, 0) + (1 - \theta)Q_{k+1}(-1, 0) = 0. \tag{11}$$

In the proof of Theorem 2.3, this relation was extended to  $t > 0$ . For odd  $k$ ,

$$\begin{aligned} Q_{k+1}(\xi, t) &= \frac{1}{2\theta - 1} [(2\theta - 1)b_{k+1}P_{k+1}(\xi) - b_{k+1}P_k(\xi)] \\ &= \frac{1}{2\theta - 1} b_{k+1} [\theta R_{k+1}^+(\xi) - (1 - \theta)R_{k+1}^-(\xi)] \\ &= \frac{b_{k+1}}{2\theta - 1} R_{k+1}^*(\xi). \end{aligned}$$

In the next section, we will compliment the pointwise observations we have made with an analysis of the constants in the dispersion and dissipation error. As shown in the literature, these are of order  $2k+$  and  $2k + 1$ , respectively. We can then extract the full  $\mathcal{O}(h^{2k+1})$  superconvergence rate using the SIAC filtering. First, we review the construction of SIAC filtering kernels.

### 2.4 Smoothness-Increasing Accuracy-Conserving (SIAC) Post-processing

The hidden local accuracy of the DG solution, discussed in the previous section, may be extracted to a global measure by applying the SIAC filter introduced by [20]. In this section, we show that superconvergent accuracy on the order of  $h^{2k+1}$  in the negative order norm, as is observed [11] for the upwind flux, still occurs when the upwind-biased DG method is used to solve linear hyperbolic conservation laws. To begin with, we observe that an error bound in the  $\mathcal{L}^2$ -norm follows from a negative order norm error estimate.

Here, we detail the component parts of the SIAC filter as defined in, for example, [11]. A B-spline  $\psi^{(\ell)}$  of order  $\ell$  is defined recursively by

$$\psi^{(1)} = \chi_{[-\frac{1}{2}, \frac{1}{2}]}; \quad \psi^{(\ell)} = \psi^{(\ell-1)} \star \chi_{[-\frac{1}{2}, \frac{1}{2}]}, \quad \ell \geq 2,$$

where  $\chi_{[-\frac{1}{2}, \frac{1}{2}]}$  is the characteristic function on the interval  $[-\frac{1}{2}, \frac{1}{2}]$  and where the operator  $\star$  denotes convolution:

$$f(x) \star g(x) = \int_{\mathbb{R}} f(x - y)g(y) dy.$$

For a multi-index  $\alpha$ , we define

$$\psi^{(\alpha)}(x) = \psi^{(\alpha_1)}(x_1) \cdots \psi^{(\alpha_d)}(x_d)$$

and, given a point  $x = (x_1, \dots, x_d) \in \mathbb{R}^d$ , we set

$$\psi^{(\ell)}(\mathbf{x}) = \psi^{(\ell)}(x_1) \cdots \psi^{(\ell)}(x_d).$$

In this way, we construct a convolution kernel

$$\mathcal{K}^{(r+1,\ell)}(\mathbf{x}) = \sum_{\gamma \in \mathbb{Z}^d} \mathbf{c}_\gamma^{r+1,\ell} \psi^{(\ell)}(\mathbf{x} - \gamma)$$

which comprises a linear combination of  $r + 1$  B-splines  $\psi^{(\ell)} \in \mathcal{C}^{\ell-2}$  of order  $\ell$  such that  $\mathcal{K}_h^{(r+1,\ell)}(x) = \frac{1}{h} \mathcal{K}\left(\frac{x}{h}\right)$  has compact support and reproduces (by convolution) polynomials of degree strictly less than  $r$ . Typically,  $r = 2k$  and  $\ell = k + 1$ , where  $k$  is the degree of the polynomial basis. In Fourier space, the kernel can be written as

$$\hat{K}(\xi) = \left( \frac{\sin\left(\frac{\xi}{2}\right)}{\frac{\xi}{2}} \right)^\ell \left( c_0 + \sum_{\gamma=0}^{\lfloor \frac{r}{2} \rfloor} c_\gamma \cos(\gamma\xi) \right) \approx 1 + \mathcal{O}(\xi^{r+1}),$$

as given in [13]. A further order of accuracy in Fourier space can be gained by requiring that the kernel is symmetric. This extra order of accuracy will only reveal itself in physical space if the negative-order norm estimates are of the same order. Notice, that the  $r + 1$  order accuracy does not rely on the smoothness,  $\ell$ , of the B-spline. The coefficients  $c_\gamma$  are tensor products of the coefficients  $c_\gamma$  found by requiring the reproduction of polynomials property  $\mathcal{K}_h^{(r+1,\ell)} \star x^p = x^p$ ,  $p < r$ , in the one-dimensional case. It is important to note that derivatives of a convolution with this kernel maybe written in terms of difference quotients:

$$D^\alpha \left( \psi_h^{(\beta)} \star v \right) = \psi_h^{(\beta-\alpha)} \star \partial_h^\alpha v, \quad \beta_i \geq \alpha_i,$$

where  $\psi_h^{(\beta)}(x) = \psi_h^{(\beta/h)} / h^d$ . Further properties of the kernel may be found in [12].

The SIAC filtered solution can be written as

$$u_h^\star(\bar{x}, t) := \mathcal{K}_h^{(r+1,\ell)}(\bar{x}) \star u_h(\bar{x}, t),$$

where the kernel has been applied by convolution at the final time. The filtered solution  $u_h^\star(x, t)$  displays increased accuracy and oscillations in the error are reduced. The results in this paper treat only the symmetric kernel where the nodes  $\gamma$  are uniformly spaced. Extension to the one-sided filter given in [11] and [20] is a straight-forward task.

### 3 Dispersion Analysis

A further approach to the analysis of these methods which has proved fruitful [6, 9, 25] in recent years involves computing the eigenstructure of the amplification matrix. The choice of initial condition and set of basis functions can be crucial in obtaining optimal results. Recent work that demonstrates the importance of this choice includes [4, 6, 23]. In what follows, we analyse the eigenvalues, which are independent of the choice of basis.

Consider the local DG solution

$$u_h(x(\xi), t)|_{I_j} = \sum_{\ell=0}^k u_j^{(\ell)}(t) \phi_j^\ell(\xi)$$

to Eq. (2) with  $d = 1$ , periodic boundary conditions and a uniform mesh and let

$$\mathbf{u}_j = \left( u_j^{(0)}, \dots, u_j^{(k)} \right)^T$$

be the coefficient vector for basis polynomials  $\phi_j^\ell(x)$  on cell  $I_j$  of degree at most  $k$ . Then, the DG scheme can be written as the following semi-discrete system of ODEs:

$$\frac{d}{dt} \mathbf{u}_j = \frac{a}{h} \left[ (A_1 + \theta A_2) \mathbf{u}_j + \theta B \mathbf{u}_{j-1} + (1 - \theta) C \mathbf{u}_{j+1} \right], \tag{12}$$

where  $A = A_1 + \theta A_2$ ,  $B$  and  $C$  are  $(k + 1) \times (k + 1)$  matrices. Note that the term  $C \mathbf{u}_{j+1}$  from the right neighbour cell is a new contribution when  $\theta < 1$ .

Continuing to follow the lines of [9, 25], the coefficient vectors can be transformed to Fourier space via the assumption

$$\mathbf{u}_j(t) = e^{i\omega x_j} \hat{\mathbf{u}}_\omega(t), \tag{13}$$

where  $\omega$  is the wave number,  $i = \sqrt{-1}$  and  $x_j = \frac{1}{2}(x_{j+\frac{1}{2}} + x_{j-\frac{1}{2}})$  is the element center, to obtain a global coefficient vector  $\hat{\mathbf{u}}_\omega$ . Substitution of the ansatz (13) into the scheme (12) gives a new ODE:

$$\frac{d}{dt} \hat{\mathbf{u}}_\omega = aG(\omega, h)\hat{\mathbf{u}}_\omega, \tag{14}$$

where

$$G(\omega, h) = \frac{1}{h} (A + \theta B e^{-i\omega h} + (1 - \theta) C e^{i\omega h})$$

is called the amplification matrix. If  $G$  is diagonalisable, then it has a full set of eigenvalues  $\lambda_1, \dots, \lambda_{k+1}$  and corresponding eigenvectors  $\Lambda_1, \dots, \Lambda_{k+1}$  and the general solution of (14) takes the form

$$\hat{\mathbf{u}}_\omega(t) = \sum_{j=1}^{k+1} C_j e^{\lambda_j t} \Lambda_j, \tag{15}$$

where the constants  $C_j, j = 1, \dots, k + 1$  depend on the initial condition. Via this approach one can inspect the size of the error and its behaviour over time as in [9, 25]. In this paper, we limit ourselves to an asymptotic expansion of the eigenvalues.

Using Mathematica to computationally perform an asymptotic analysis on  $\zeta = \omega h = 0$ , we can obtain the following sets of eigenvalues  $\lambda_j$  of the amplification matrices  $G$  for the cases  $k = 0, 1, 2, 3$ . For

$$\begin{aligned} k = 0 : \lambda_1 &= -i\omega - \frac{1}{2}(2\theta - 1)\omega^2 h + \mathcal{O}(h^2); \\ k = 1 : \begin{cases} \lambda_1 &= -i\omega - \frac{1}{72} \frac{1}{2\theta - 1} \omega^4 h^3 - \frac{i}{270} \frac{1 + 6\theta - 6\theta^2}{(1 - 2\theta)^2} \omega^5 h^4 + \mathcal{O}(h^5), \\ \lambda_2 &= -\frac{6(2\theta - 1)}{h} + 3i\omega + (2\theta - 1)\omega^2 h + \mathcal{O}(h^2); \end{cases} \\ k = 2 : \begin{cases} \lambda_1 &= -i\omega - \frac{2\theta - 1}{7200} \omega^6 h^5 + \frac{i}{300} \left( \theta^2 - \theta + \frac{1}{14} \right) \omega^7 h^6 + \mathcal{O}(h^7), \\ \lambda_{2,3} &= -\frac{3(2\theta - 1)}{h} \pm i\sqrt{51 + 36\theta - 36\theta^2} \omega + \mathcal{O}(h). \end{cases} \end{aligned}$$

For the case  $k = 3$ , the algebra involved in computing the roots of  $R_{k+1}^*$  and in computing the eigenvalues of the amplification matrix becomes prohibitively substantial and the need to evaluate components numerically makes it particularly difficult to obtain tidy closed expressions for the coefficients. For  $k = 3$ , we have found that one eigenvalue satisfies

$$\lambda_1 = -i\omega - \frac{3.125 \times 10^{-4}}{441(2\theta - 1)}\omega^8 h^7 - \frac{1.25 \times 10^{-3}}{27783} \frac{19 - 48\theta + 28\theta^2}{(1 - 2\theta)^2} \omega^9 h^8 + \mathcal{O}(h^9)$$

while the leading order term of the other eigenvalues has a negative real part on the order of  $\frac{1}{h}$ .

For each value of  $k$ , the eigenvalue  $\lambda_1$  has physical relevance, approximating  $-i\omega$  with dispersion error on the order of  $h^{2k+1}$  and dissipation error on the order of  $h^{2k+2}$ . This is consistent with the previous findings of [3, 9, 10, 19, 21, 25]. The coefficient of the leading order real term of the physically relevant eigenvalues  $\lambda_1$  is negative. While for even  $k$  this coefficient vanishes in the limit  $\theta \rightarrow \frac{1}{2}$ , for odd  $k$ , due to the factor  $(2\theta - 1)^{-1}$ , it grows without bound with reducing values of  $\theta$ . This (blow-up) behaviour is amplified in the coefficient of  $h^{2k+2}$ . Note that such differences between odd and even  $k$  do not manifest when  $\theta = 1$  since then  $2\theta - 1 = 1$ .

The remaining eigenvalues are non-physically relevant but have negative real part on the order of  $\frac{1}{h}$  so that the corresponding eigenvectors in the solution (15) are sufficiently damped over time. This dampening is observed to be slower in the cases  $k = 1, 2$  for lower values of  $\theta$  [6].

**Remark 3.1** While the eigenvalues are independent of the choice of basis functions, one must make an appropriate choice of the interpolating initial condition and basis functions to extract superconvergent accuracy in the eigenvectors. If one uses a Lagrange–Radau basis on roots of  $R_{k+1}^+(\xi)$ , the appropriate choice when  $\theta = 1$ , in the case  $k = 1$  the physically relevant eigenvector satisfies

$$C_1 \Lambda_1 - \hat{u}(0) = \left[ \begin{array}{l} -\frac{1-\theta}{18(1-2\theta)}\omega^2 h^2 + \frac{11-11\theta+2\theta^2}{324(1-2\theta)^2} i\omega^3 h^3 + \mathcal{O}(h^4) \\ -\frac{1-\theta}{6(1-2\theta)}\omega^2 h^2 + \frac{1-25\theta+22\theta^2}{108(1-2\theta)^2} i\omega^3 h^3 + \mathcal{O}(h^4) \end{array} \right],$$

while similarly the non-physically relevant eigenvector satisfies

$$C_2 \Lambda_2 = \left[ \begin{array}{l} \frac{1-\theta}{18(1-2\theta)}\omega^2 h^2 - \frac{11-11\theta+2\theta^2}{324(1-2\theta)^2} i\omega^3 h^3 + \mathcal{O}(h^4) \\ -\frac{1-\theta}{6(1-2\theta)}\omega^2 h^2 - \frac{1-25\theta+22\theta^2}{108(1-2\theta)^2} i\omega^3 h^3 + \mathcal{O}(h^4) \end{array} \right].$$

The leading order terms vanish only when  $\theta = 1$  when the interpolation points coincide with the superconvergent points of the scheme. Numerical results suggest that for  $k = 2$ , when we have  $k + 1$  roots of  $R_{k+1}^*(\xi)$ , we are able to obtain the optimal  $\mathcal{O}(h^{2k+1})$  accuracy using  $u_h(x, 0) = \pi_{k+1}^* u_0(x)$ .

### 4 Extracting Superconvergence

To investigate the SIAC filtered error, denote by  $e_h = u - u_h$  the usual DG error and let

$$u_h^* = \mathcal{K}_h^{(2k+1,k+1)} \star u_h$$

be the DG solution to Eq. (2) post-processed by convolution kernel. We have the following estimate:

**Theorem 4.1** *Let  $u_h$  be the numerical solution to the linear hyperbolic conservation law (2) with the smooth initial condition obtained via a DG scheme (4) with upwind-biased flux. Then,*

$$\|u - u_h^*\|_0 = \|u - \mathcal{K}_h \star u\|_0 + \|\mathcal{K}_h \star u - u_h^*\|_0 \leq C(u_0, \theta, T)h^{2k+1} \tag{16}$$

for  $r = 2k$  and  $\ell = k + 1$ .

The first term on the right-hand side of (16) is bounded by  $Ch^{r+1}$  from the integral form of Taylor’s theorem and from the reproduction of polynomials property of the convolution (Lemma 5.1, [11]). Thus we need only to consider the second term for which

$$\begin{aligned} \|\mathcal{K}_h \star u - u_h^*\|_0 &= \|\mathcal{K}_h \star e_h\|_0 \leq \sum_{|\alpha| \leq \ell} \|D^\alpha(\mathcal{K}_h \star e_h)\|_0 \\ &\leq \sum_{|\alpha| \leq \ell} \|\tilde{\mathcal{K}}_h\|_1 \|\partial_h^\alpha e_h\|_{-\ell} \end{aligned} \tag{17}$$

by kernel properties of the  $\alpha$ th derivative  $D^\alpha$ , the kernel’s relation to the divided difference  $\partial^\alpha$  and by Young’s inequality for convolutions. The tilde on  $\tilde{\mathcal{K}}_h$  in inequality (17) signals that the kernel uses  $\psi^{(\ell-\alpha)}$ , which is a result of the property  $D^\alpha \psi^{(\ell)} = \partial_h^\alpha \psi^{(\ell-\alpha)}$ .

Note that  $\|\tilde{\mathcal{K}}_h\|_\ell = \sum_{i=0}^r |c_i|$  is just the sum of the kernel coefficients so we only need to show that  $\|\partial_h^\alpha e_h\|_{-\ell} \leq Ch^{2k+1}$ . Furthermore, the formulation of the DG scheme for the solution is similar to that for the divided differences and, as speculated in [7],

$$\|\partial_h^\alpha(u - u_h)\|_{-\ell, \Omega} \leq C\|\partial_h^\alpha u_0\|_{\ell, \Omega} h^{2k+m}, \quad m \in \{0, 1/2, 1\}. \tag{18}$$

This allows us to only have to consider the negative order norm of the solution itself; superconvergent accuracy in the negative order norm gives superconvergent accuracy in the  $\mathcal{L}^2$ -norm for the post-processed solution. The following result provides the required negative order norm error estimate.

**Remark 4.1** Notice that the superconvergent points for the upwind-biased scheme, as described in the one-dimensional case in Lemma 2.2, change with the value of  $\theta$ . However, the global superconvergence in the negative-order norm occurs regardless of the value of  $\theta$ .

**Theorem 4.2** *Let  $u_h$  be the numerical solution to the linear hyperbolic conservation law (2) with the smooth initial condition obtained via a DG scheme (4) with the upwind-biased flux. Then,*

$$\left| \partial_h^\alpha(u - u_h)(T) \right|_{-\ell, \Omega} \leq C(u_0, \theta, T)h^{2k+1}, \quad \alpha < \ell. \tag{19}$$

**Proof** For simplicity, we consider the case when  $\alpha = 0$ . The case for  $\alpha > 0$  is similar [22]. To extract information about the error at the final time, we work with the dual equation: find a continuous and analytic  $\phi(\mathbf{x}, t)$  such that

$$\phi_t + \sum_{i=1}^d a_i \phi_{x_i} = 0; \quad \phi(\mathbf{x}, T) = \Phi(\mathbf{x}), \quad (\mathbf{x}, t) \in \Omega \times [0, T]. \tag{20}$$

If we test Eq. (20) against the solution  $u$  to the original system (2) and, similarly, multiply the original system by  $\phi$  and integrate over the domain, integrating by parts and adding the two new equations yields

$$\frac{d}{dt}(u, \phi)_\Omega = 0.$$

A periodicity relation is obtained by integrating with respect to  $t$  and appealing to the Fundamental Theorem of Calculus:

$$(u(T), \Phi)_\Omega = (u, \phi)_\Omega(T) = (u, \phi)_\Omega(0) = (u_0, \phi(0))_\Omega.$$

On the other hand, we can write instead

$$(u_h(T), \Phi)_\Omega = (u_h, \phi)_\Omega(T) = \int_0^T \frac{d}{dt}(u_h, \phi)_\Omega dt + (u_h, \phi)_\Omega(0).$$

Thus, we can estimate the term appearing in the definition of the negative order norm:

$$(e, \Phi)_\Omega(T) = (e, \phi)_\Omega(0) - \int_0^T \frac{d}{dt}(u_h, \phi) dt. \tag{21}$$

Information about the model problem and the method can be incorporated into the second term on the right-hand side of Eq. (21) using the DG formulation and the dual equation:

$$\begin{aligned} \frac{d}{dt}(u_h, \phi)_\Omega &= ((u_h)_t, \phi)_\Omega + (u_h, \phi_t)_\Omega \\ &= ((u_h)_t, \phi - \chi)_\Omega + ((u_h)_t, \chi)_\Omega + (u_h, \phi_t)_\Omega \\ &= ((u_h)_t, \phi - \chi)_\Omega - B(u_h, \chi) + (u_h, \phi_t)_\Omega \\ &= ((u_h)_t, \phi - \chi)_\Omega + B(u_h, \phi - \chi) - B(u_h, \phi) + (u_h, \phi_t)_\Omega, \quad \chi \in V_h^k. \end{aligned} \tag{22}$$

Hence we can rewrite Eq. (21) as

$$(u - u_h, \Phi)_\Omega(T) = \Theta_1 + \Theta_2 + \Theta_3, \tag{23}$$

where



$$\begin{cases} \Theta_1 = (u - u_h, \phi)_{\Omega}(0); \\ \Theta_2 = - \int_0^T [((u_h)_t, \phi - \chi)_{\Omega} + B(u_h, \phi - \chi)] dt; \\ \Theta_3 = - \int_0^T [(u_h, \phi_t)_{\Omega} - B(u_h, \phi)] dt \end{cases} \tag{24}$$

with

$$\begin{cases} |\Theta_1| \leq C_1 h^{2k+2} \|u_0\|_{k+1} \|\phi(0)\|_{k+1}, \\ |\Theta_3| = \left| \int_0^T (u_h, \phi_t)_{\Omega} - B(u_h, \phi) dt \right| = 0, \end{cases} \tag{25}$$

where this last equality follows by using the properties of the dual equation and the single-valued flux, together with  $\phi$  being continuous. Notice that the terms on the right-hand side of Eq. (23) can be estimated individually and are similar to those presented in [7, 11], here we only elaborate on contribution of the flux,  $\Theta_2$ .

In contrast to  $\Theta_1$  and  $\Theta_3$ , estimation of the  $\Theta_2$  term is affected by the choice of the flux parameter  $\theta$ . Let  $\mathbb{P}_h \phi$  be the projection onto the approximation space. Then since the projection error  $\phi - \mathbb{P}_h \phi$  is orthogonal to the approximation space, we can write

$$\begin{aligned} |\Theta_2| &= \left| \int_0^T B(u_h; \phi - \mathbb{P}_h \phi) dt \right| \\ &\leq C_a \left( \frac{1}{h} \int_0^T \| \llbracket u_h \rrbracket \|_{\Omega}^2 dt \right)^{1/2} \left( \int_0^T \| \phi - \mathbb{P}_h \phi \|^2_{\mathbf{R}} dt \right)^{1/2} \\ &\quad + (1 - \theta) C_a \left( \frac{1}{h} \int_0^T \| \llbracket u_h \rrbracket \|_{\Omega}^2 dt \right)^{1/2} \left( \frac{1}{h} \int_0^T \| \llbracket \phi - \mathbb{P}_h \phi \rrbracket \|_{\partial \Omega}^2 dt \right)^{1/2} \tag{26} \\ &\leq C_a \left( C_u \frac{1}{h} h^{2(k+1)} \right)^{1/2} \left[ C_q h^{k+\frac{1}{2}} \|\phi\|_{k+1} + C_p (1 - \theta) h^{k+\frac{1}{2}} \|\phi\|_{k+1} \right] \\ &= C_a C_u [C_q + (1 - \theta) C_p] h^{2k+1} \|\phi\|_{k+1}(T) \\ &= C_2 h^{2k+1} \|\Phi\|_{k+1}, \end{aligned}$$

where the constant  $C_2 = C_2^+ + (1 - \theta) C_2^-$  depends on  $\theta$ .

Combining the estimates and using the periodicity of the boundary conditions, we conclude with a bound on the numerator in the definition of the negative order norm:

$$\begin{aligned} (u - u_h, \Phi)_{\Omega}(T) &= \Theta_1 + \Theta_2 + \Theta_3 \\ &\leq C_1 h^{2k+2} \|u_0\|_{k+1} \|\phi(0)\|_{k+1} + C_2 h^{2k+1} \|\Phi\|_{k+1}. \end{aligned} \tag{27}$$

Inserting the inequality into the definition of the negative order norm completes the proof of Theorem 4.2.

**Remark 4.2** The effect of the introduction in the flux function of the parameter  $\theta$  is limited to a contribution to the constant attached to the order term in the negative order norm error estimate. This is in contrast to the changing local behaviour seen in the pointwise analysis in Sect. 2.3. Despite the observations of Remark 2.4 regarding the local behaviour when  $k$  is odd, we can extract the same global order of accuracy,  $\mathcal{O}(h^{2k+1})$ , for any polynomial degree  $k$ .

### 5 Numerical Experiments

We present a numerical discussion for the test equation

$$\begin{aligned} u_t + u_x &= 0, & (x, t) \in [0, 2\pi] \times (0, T), \\ u(x, 0) &= \sin(x), & u(0, T) = u(2\pi, T). \end{aligned}$$

Figures 1, 2 and 3 show the DG discretisation errors on a grid of  $N = 10$  elements for various values of  $\theta$  and for polynomial degrees  $k = 1, 2, 3, 4$ . Marked by the red crosses are the theoretical superconvergent points which are roots of  $R_{k+1}^*(\xi)$  and which change with the value of  $\theta \in (\frac{1}{2}, 1]$ . The error curves cross the zero axis near these roots. In [2], Adj-erid et al. commented that the intersection points align more closely as  $k$  increases and we observe that here as well.

For  $k = 2$  we observe  $k + 1$  superconvergent points while for  $k = 1$  and  $k = 3$ , in general, the error curves cross the zero axis only  $k$  times. Furthermore, as the value of  $\theta$  reduces, we see an overall reduction in the magnitude of the errors for  $k = 2$ . On the other hand, when  $k = 1$  or  $k = 3$  the magnitude of the errors in general increases for smaller values of  $\theta$ .

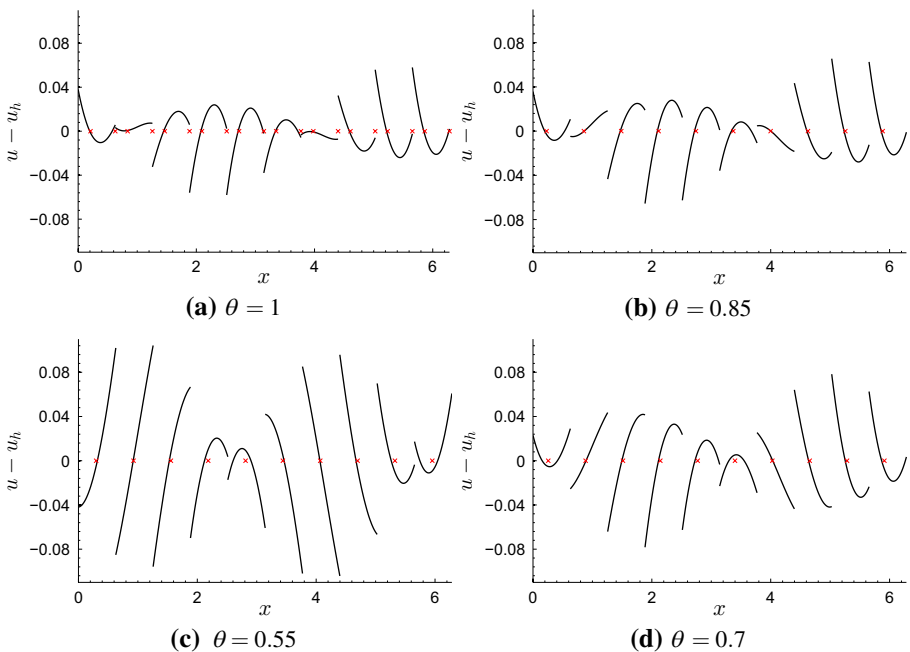


**Fig. 1** Discretisation errors for DG solution to 1D linear hyperbolic equation with  $k = 1$  and  $N = 10$

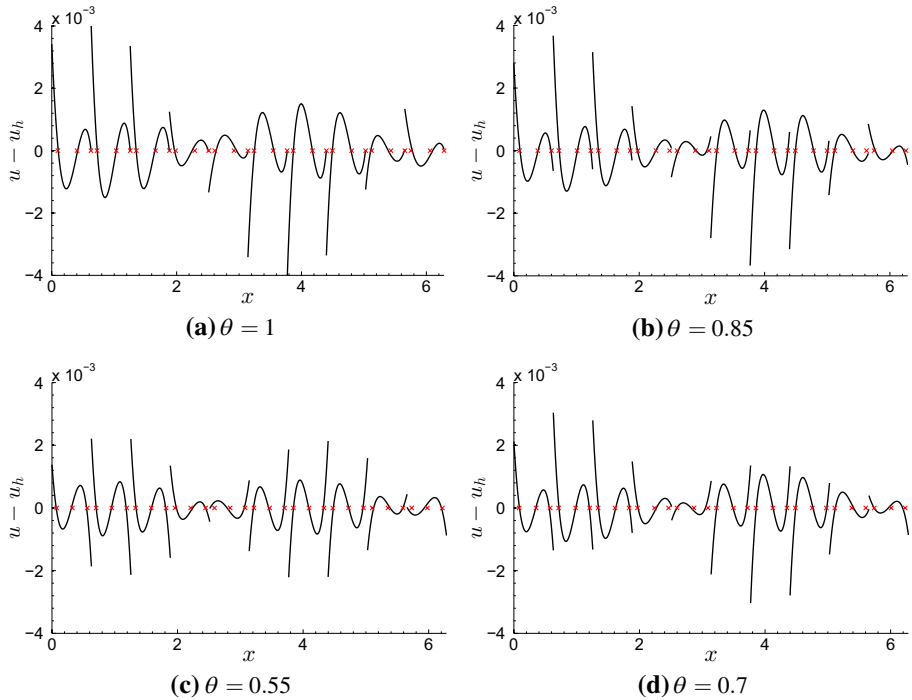


**Fig. 2** Discretisation errors for DG solution to 1D linear hyperbolic equation with  $k = 2$  and  $N = 10$

Inside certain anomalous elements, for example the fifth and tenth elements in Fig. 2, the curves miss the crosses or, as in the sixth element in Fig. 3, we observe an additional intersection and this may be due to the initial condition  $\sin(x)$ .

Tables 2, 3 and 4 illustrate the order  $h^{k+1}$  accuracy of the DG solution in the  $\mathcal{L}^2$ - and  $\mathcal{L}^\infty$ -norms. After post-processing by the SIAC filter, we observe the  $\mathcal{O}(h^{2k+1})$  accuracy in the  $\mathcal{L}^2$ -norm described in Sect. 4 and we also see  $\mathcal{O}(h^{2k+1})$  accuracy in the  $\mathcal{L}^\infty$ -norm.

For odd  $k$ , convergence to the expected orders is slower for lower values of  $\theta$  but is eventually achieved. Furthermore, if one compares the same degrees of mesh refinement for decreasing values of  $\theta$ , one observes increasing errors for  $k = 1, 3$  and reducing errors for  $k = 2$ . For the post-processed solution, this is due in large part to the contribution of  $\theta$  to the constant attached to the order term in the error estimate of Theorem 4.2.

The highly oscillatory nature of the DG solution, indicating the existence of the hidden superconvergent points, can be seen in Figs. 4, 5, 6, 7, 8, 9, 10, 11, 12, 13, 14 and 15 alongside the post-processed solutions which have increased smoothness and improved accuracy. The reduced numerical viscosity enforced by the upwind-biased flux is evident when comparing plots for  $\theta = 1$  and  $\theta = 0.55$ .

**Remark 5.1** For one-dimensional nonlinear hyperbolic scalar equations and systems, results using the Lax–Friedrichs flux can be found in [16, 17]. The theoretical extension to multi-dimensional nonlinear hyperbolic equations is quite difficult to obtain as they rely on divided difference estimates.

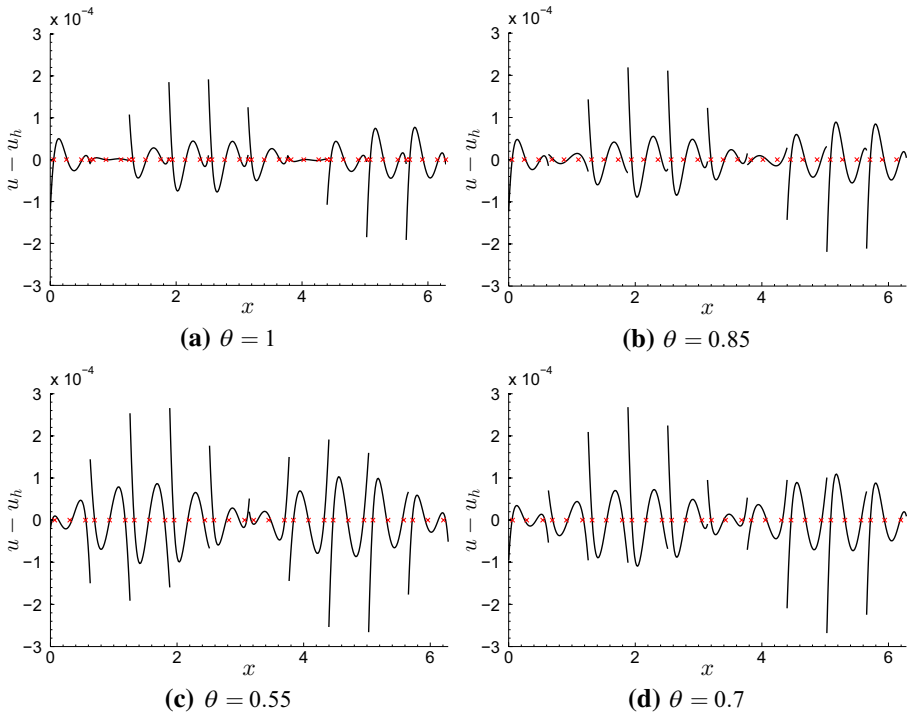


**Fig. 3** Discretisation errors for DG solution to 1D linear hyperbolic equation with  $k = 3$  and  $N = 10$

**Table 2**  $\mathcal{L}^2$ - and  $\mathcal{L}^\infty$ -norms of errors before and after post-processing for case  $k = 1$

Mesh	$\mathcal{P}^1$ : Before filter				$\mathcal{P}^1$ : After filter			
	$\mathcal{L}^2$ error	Order	$\mathcal{L}^\infty$ error	Order	$\mathcal{L}^2$ error	Order	$\mathcal{L}^\infty$ error	Order
$\theta = 1$								
10	1.64E-02	–	4.98E-02	–	3.46E-03	–	5.05E-03	–
20	4.21E-03	1.96	1.36E-02	1.86	3.72E-04	3.22	5.39E-04	3.22
40	1.05E-03	1.99	3.50E-03	1.95	4.23E-05	3.13	6.07E-05	3.13
80	2.65E-04	1.99	8.85E-04	1.98	5.02E-06	3.07	7.17E-06	3.08
$\theta = 0.85$								
10	1.96E-02	–	5.71E-02	–	4.01E-03	–	5.93E-03	–
20	5.29E-03	1.88	1.63E-02	1.80	4.75E-04	3.07	6.91E-04	3.10
40	1.35E-03	1.96	4.27E-03	1.93	5.72E-05	3.05	8.22E-05	3.07
80	3.40E-04	1.99	1.08E-03	1.97	6.99E-06	3.03	9.95E-06	3.04
$\theta = 0.55$								
10	4.14E-02	–	9.80E-02	–	6.58E-03	–	9.75E-03	–
20	1.61E-02	1.36	3.71E-02	1.40	1.29E-03	2.34	1.87E-03	2.37
40	5.91E-03	1.44	1.42E-02	1.58	2.37E-04	2.44	3.39E-04	2.46
80	1.86E-03	1.66	4.56E-03	1.64	3.82E-05	2.63	5.44E-05	2.64

**Table 3**  $\mathcal{L}^2$ - and  $\mathcal{L}^\infty$ -norms of errors before and after post-processing for case  $k = 2$

Mesh	$\mathcal{P}^2$ : Before filter				$\mathcal{P}^2$ : After filter			
	$\mathcal{L}^2$ error	Order	$\mathcal{L}^\infty$ error	Order	$\mathcal{L}^2$ error	Order	$\mathcal{L}^\infty$ error	Order
$\theta = 1$								
10	8.59E-04	–	3.02E-03	–	1.43E-04	–	2.04E-04	–
20	1.06E-04	3.00	3.66E-03	3.04	2.52E-06	5.83	3.85E-06	5.83
40	1.33E-05	2.99	4.62E-05	2.98	4.46E-08	5.81	6.34E-08	5.82
80	1.67E-06	2.99	5.78E-06	2.99	8.53E-09	5.71	1.21E-09	5.71
$\theta = 0.85$								
10	7.35E-04	–	2.61E-03	–	1.41E-04	–	2.01E-04	–
20	9.03E-05	3.02	3.10E-04	3.07	2.44E-06	5.86	3.47E-06	5.86
40	1.12E-05	3.00	3.85E-05	3.00	4.19E-08	5.86	5.95E-08	5.86
80	1.40E-06	3.00	4.81E-06	3.00	7.66E-10	5.77	1.08E-09	5.77
$\theta = 0.55$								
10	5.66E-04	–	1.46E-03	–	1.36E-03	–	1.93E-04	–
20	6.97E-05	3.01	1.86E-04	2.97	2.26E-06	5.91	3.20E-06	5.91
40	8.70E-06	3.00	2.31E-05	3.00	3.63E-08	5.95	5.15E-08	5.96
80	1.08E-06	3.00	2.87E-06	3.01	5.91E-10	5.94	8.39E-10	5.93

**Table 4**  $\mathcal{L}^2$ - and  $\mathcal{L}^\infty$ -norms of errors before and after post-processing for case  $k = 3$

Mesh	$\mathcal{P}^3$ : Before filter				$\mathcal{P}^3$ : After filter			
	$\mathcal{L}^2$ error	Order	$\mathcal{L}^\infty$ error	Order	$\mathcal{L}^2$ error	Order	$\mathcal{L}^\infty$ error	Order
$\theta = 1$								
10	2.35E-04	–	1.91E-04	–	1.61E-05	–	2.28E-05	–
20	1.30E-05	4.16	1.06E-05	4.16	6.97E-08	7.86	9.81E-08	7.86
40	8.67E-07	3.91	7.33E-07	3.86	3.34E-10	7.69	4.72E-10	7.69
$\theta = 0.85$								
10	2.74E-04	–	2.18E-04	–	1.61E-05	–	2.28E-05	–
20	1.63E-05	4.06	1.31E-05	4.06	6.94E-08	7.86	9.82E-08	7.86
40	1.07E-06	3.92	8.81E-07	3.89	3.34E-10	7.69	4.73E-10	7.69
$\theta = 0.55$								
10	4.04E-04	–	2.65E-04	–	1.61E-05	–	2.28E-05	–
20	4.99E-05	3.01	3.22E-05	3.04	6.96E-08	7.85	9.85E-08	7.85
40	4.72E-06	3.40	2.97E-06	3.43	3.39E-10	7.68	4.80E-10	7.68

## 6 Conclusions

In this article, we have discussed the effect of the choice of the flux on three types of superconvergence: pointwise, wave propagation properties, and the negative-order norm. We specifically provide an explicit formula for the form of the error constant for the dispersion and dissipation errors. We illustrated this effect through the use of the

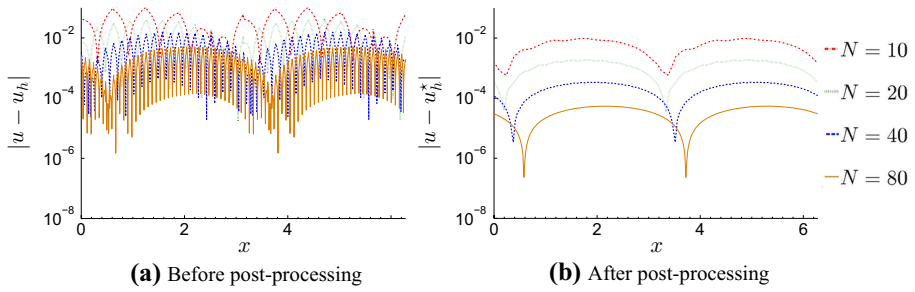


Fig. 4  $\theta = 1$

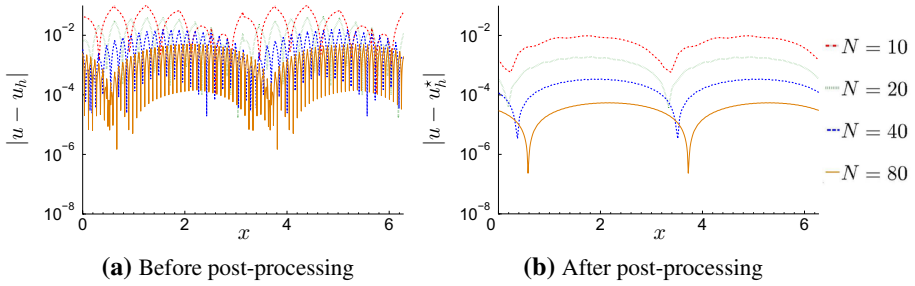


Fig. 5  $\theta = 0.85$

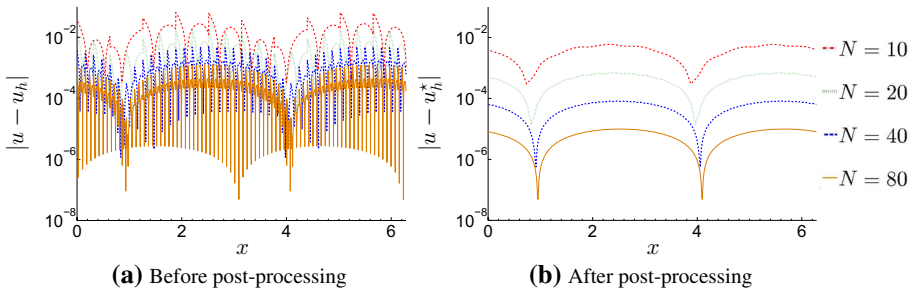


Fig. 6  $\theta = 0.55$

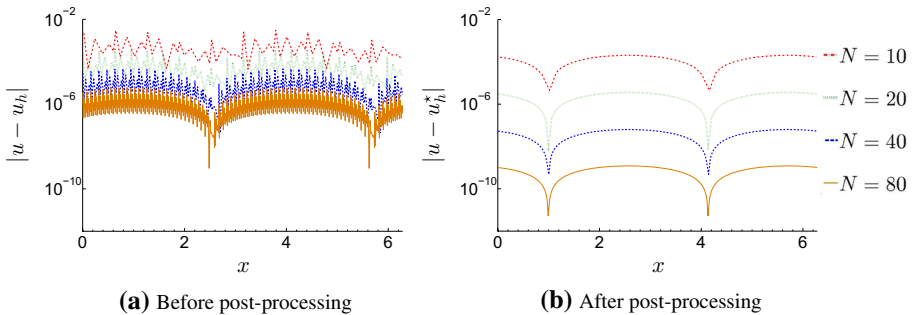


Fig. 7  $\theta = 1$

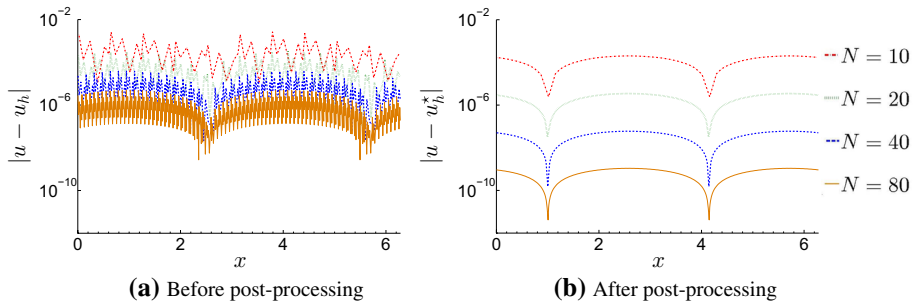


Fig. 8  $\theta = 0.85$

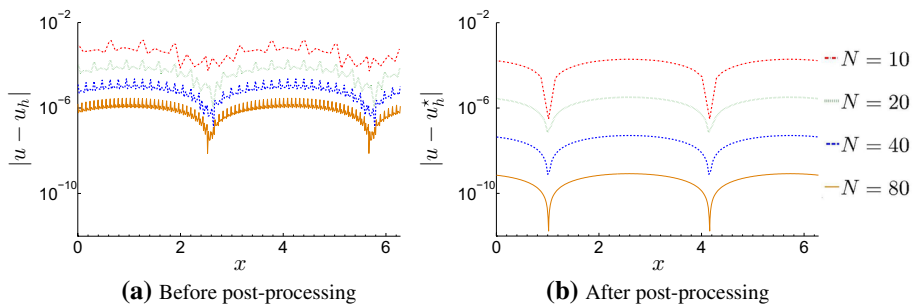


Fig. 9  $\theta = 0.55$

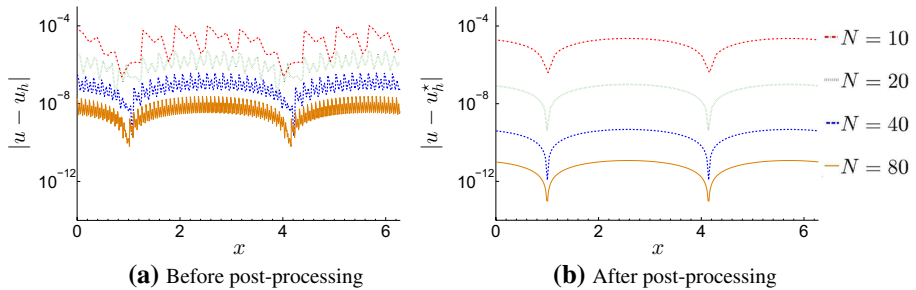


Fig. 10  $\theta = 1$

upwind-biased flux which takes a convex combination of left and right approximation values. By exploring the error constant in the dissipation and dispersion errors, we are able to better understand why it is important to take a more central flux for even degree polynomial degree approximations and a more upwind flux for odd degree polynomial

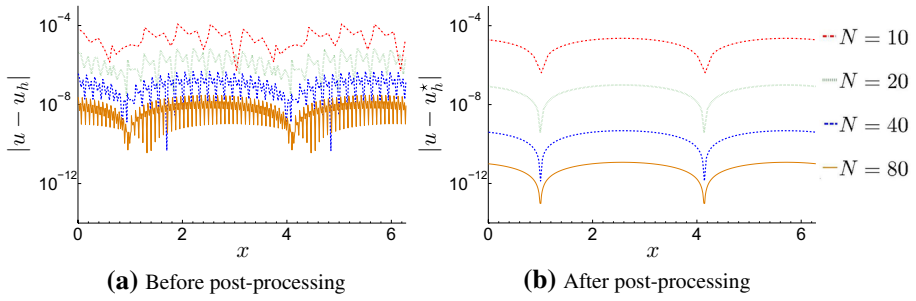


Fig. 11  $\theta = 0.85$

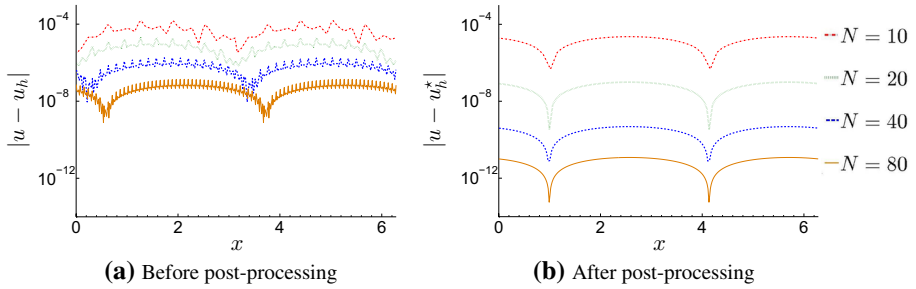


Fig. 12  $\theta = 0.55$

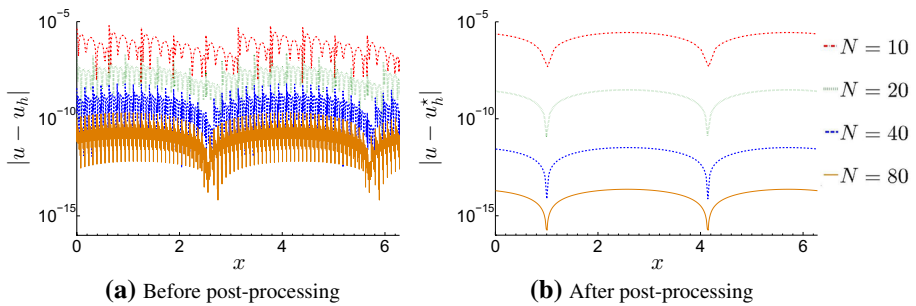


Fig. 13  $\theta = 1$

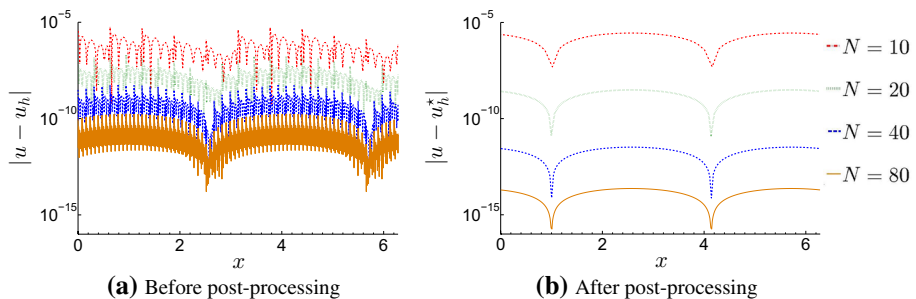


Fig. 14  $\theta = 0.85$



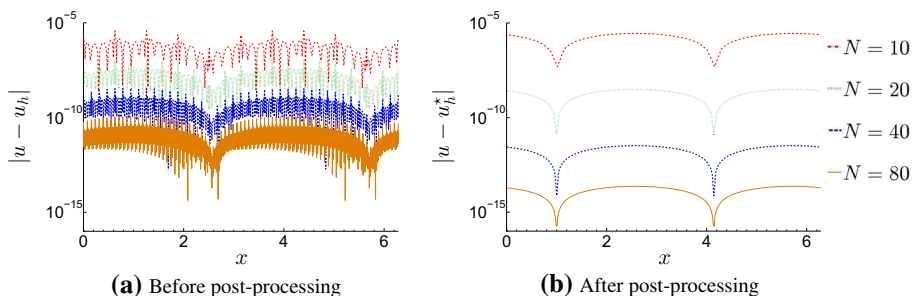


Fig. 15  $\theta = 0.55$

approximations. We also proved that the superconvergent extraction capabilities of the SIAC filter are unaffected. Numerical results were presented to confirm our findings.

**Acknowledgements** This work was sponsored by the Air Force Office of Scientific Research (AFOSR), Air Force Material Command, USAF, under grant number FA8655-09-1-3017. The U.S. Government is authorized to reproduce and distribute reprints for Governmental purposes notwithstanding any copyright notation thereon.

## Compliance with ethical standards

**Conflict of interest** On behalf of all authors, the Jennifer K. Ryan states that there is no conflict of interest.

**Open Access** This article is licensed under a Creative Commons Attribution 4.0 International License, which permits use, sharing, adaptation, distribution and reproduction in any medium or format, as long as you give appropriate credit to the original author(s) and the source, provide a link to the Creative Commons licence, and indicate if changes were made. The images or other third party material in this article are included in the article's Creative Commons licence, unless indicated otherwise in a credit line to the material. If material is not included in the article's Creative Commons licence and your intended use is not permitted by statutory regulation or exceeds the permitted use, you will need to obtain permission directly from the copyright holder. To view a copy of this licence, visit <http://creativecommons.org/licenses/by/4.0/>.

## References

1. Adjerid, S., Baccouch, M.: A superconvergent local discontinuous Galerkin method for elliptic problems. *J. Sci. Comput.* **52**(1), 113–152 (2012)
2. Adjerid, S., Devine, K.D., Flaherty, J.E., Krivodonova, L.: A posteriori error estimation for discontinuous Galerkin solutions of hyperbolic problems. *Comput. Methods Appl. Mech. Eng.* **191**(11), 1097–1112 (2002)
3. Ainsworth, M.: Dispersive and dissipative behaviour of high order discontinuous Galerkin finite element methods. *J. Comput. Phys.* **198**(1), 106–130 (2004)
4. Cao, W., Zhang, Z., Zou, Q.: Superconvergence of discontinuous Galerkin methods for linear hyperbolic equations. *SIAM J. Numer. Anal.* **52**(5), 2555–2573 (2014)
5. Cao, W., Li, D., Yang, Y., Zhang, Z.: Superconvergence of discontinuous Galerkin methods based on upwind-biased fluxes for 1D linear hyperbolic equations. *ESAIM Math. Model. Numer. Anal.* **51**(2), 467–486 (2017)
6. Cheng, Y., Chou, C.-S., Li, F., Xing, Y.:  $L^2$  stable discontinuous Galerkin methods for one-dimensional two-way wave equations. *Math. Comput.* **86**, 121–155 (2014)

7. Cockburn, B., Luskin, M., Shu, C.-W., Süli, E.: Enhanced accuracy by post-processing for finite element methods for hyperbolic equations. *Math. Comput.* **72**(242), 577–606 (2003)
8. Cockburn, B., Shu, C.-W.: TVB Runge–Kutta local projection discontinuous Galerkin finite element method for conservation laws. ii. General framework. *Math. Comput.* **52**(186), 411–435 (1989)
9. Guo, W., Zhong, X., Qiu, J.-M.: Superconvergence of discontinuous Galerkin and local discontinuous Galerkin methods: eigen-structure analysis based on Fourier approach. *J. Comput. Phys.* **235**, 458–485 (2013)
10. Hu, F.Q., Atkins, H.L.: Eigensolution analysis of the discontinuous Galerkin method with nonuniform grids: I. One space dimension. *J. Comput. Phys.* **182**(2), 516–545 (2002)
11. Ji, L., van Slingerland, P., Ryan, J., Vuik, K.: Superconvergent error estimates for position-dependent smoothness-increasing accuracy-conserving (SIAC) post-processing of discontinuous Galerkin solutions. *Math. Comput.* **83**(289), 2239–2262 (2014)
12. Ji, L., Xu, Y., Ryan, J.K.: Accuracy-enhancement of discontinuous Galerkin solutions for convection–diffusion equations in multiple-dimensions. *Math. Comput.* **81**(280), 1929–1950 (2012)
13. Ji, L., Ryan, J.K.: Smoothness-increasing accuracy-conserving (SIAC) filters in Fourier space. In: Kirby, R.M., Berzins, M., Hesthaven, J.S. (eds.) *Spectral and High Order Methods for Partial Differential Equations ICOSAHOM 2014*, pp. 415–423. Springer, Cham (2015)
14. Krivodonova, L., Qin, R.: An analysis of the spectrum of the discontinuous Galerkin method. *Appl. Numer. Mathematics* **64**, 1–18 (2013)
15. Meng, X., Shu, C.-W., Wu, B.: Optimal error estimates for discontinuous Galerkin methods based on upwind-biased fluxes for linear hyperbolic equations. *Math. Comput.* **85**, 1225–1261 (2016)
16. Meng, X., Ryan, J.K.: Discontinuous Galerkin methods for nonlinear scalar hyperbolic conservation laws: divided difference estimates and accuracy enhancement. *Numer. Math.* **136**(1), 27–73 (2017)
17. Meng, X., Ryan, J.K.: Divided difference estimates and accuracy enhancement of discontinuous Galerkin methods for nonlinear symmetric systems of hyperbolic conservation laws. *IMA J. Numer. Anal.* **38**(1), 125–155 (2017)
18. Ryan, J.K., Shu, C.-W., Atkins, H.: Extension of a post processing technique for the discontinuous Galerkin method for hyperbolic equations with application to an aeroacoustic problem. *SIAM J. Sci. Comput.* **26**(3), 821–843 (2005)
19. Sherwin, S.: Dispersion analysis of the continuous and discontinuous Galerkin formulations. In: Cockburn B., Karniadakis G.E., Shu C.-W. (eds) *Discontinuous Galerkin Methods*, pp. 425–431. Springer, Berlin (2000)
20. Van Slingerland, P., Ryan, J.K., Vuik, C.: Position-dependent smoothness-increasing accuracy-conserving (SIAC) filtering for improving discontinuous Galerkin solutions. *SIAM J. Sci. Comput.* **33**(2), 802–825 (2011)
21. Yang, H., Li, F., Qiu, J.: Dispersion and dissipation errors of two fully discrete discontinuous Galerkin methods. *J. Sci. Comput.* **55**(3), 552–574 (2013)
22. Yang, Y., Shu, C.-W.: Discontinuous Galerkin method for hyperbolic equations involving  $\delta$ -singularities: negative-order norm error estimates and applications. *Numer. Math.* **124**(4), 753–781 (2013)
23. Yang, Y., Shu, C.-W.: Analysis of optimal superconvergence of discontinuous Galerkin method for linear hyperbolic equations. *SIAM J. Numer. Anal.* **50**(6), 3110–3133 (2012)
24. Zhang, M., Shu, C.-W.: An analysis of three different formulations of the discontinuous Galerkin method for diffusion equations. *Math. Models Methods Appl. Sci.* **13**(03), 395–413 (2003)
25. Zhong, X., Shu, C.-W.: Numerical resolution of discontinuous Galerkin methods for time dependent wave equations. *Comput. Methods Appl. Mech. Eng.* **200**(41), 2814–2827 (2011)